On the Performance of Graphene-Based D-Shaped Photonic Crystal Fibre Biosensor Using Surface Plasmon Resonance

Jitendra Narayan Dash · Rajan Jha

Abstract We propose a D-shaped photonic crystal fibre-based surface plasmon resonance sensor considering graphene on silver for sensing of refractive index of analyte and thickness of biolayer. The different structural and material parameters associated with sensor have been optimised. Graphene not only helps in adsorption of biomolecules due to π-π stacking interaction but at the same time prevents oxidation of metal-like silver. Numerical simulation shows that amplitude sensitivity of the proposed structure for chemical analytes is 216 RIU^{-1} (refractive index unit) with a resolution of 4.6×10^{-5} RIU while the wavelength sensitivity of the proposed sensor is found to be as high as 3700 nm RIU^{-1} with resolution of 2.7×10^{-5} RIU. Further, the proposed sensor can also be used for the detection of biolayer thickness in both amplitude and wavelength interrogations. An amplitude sensitivity of 0.26 nm^{-1} with resolution of 39 pm and wavelength sensitivity of 2 nm nm^{-1} with resolution of 50 pm is achievable for the determination of biolayer thickness. The proposed structure is easy to use as there is no need of filling of voids, and the analytes can be placed easily on the flat surface of photonic crystal fibre (PCF).

Keywords Surface plasmon resonance · Sensor · Photonic crystal fibre (PCF) · Sensitivity

J. N. Dash · R. Jha (✉)
Nanophotonics and Plasmonics Laboratory, School of Basic Sciences, Indian Institute of Technology Bhubaneswar, Toshali Bhawan, Bhubansewar, Odisha, India
e-mail: rjha@iitbbs.ac.in

R. Jha
e-mail: rajaniitd@gmail.com

Introduction

Collective oscillation of electrons at the metal dielectric interface due to the incident electromagnetic wave is called surface plasmon wave. When the wave vector of incident field matches with the wave vector of surface plasmon, there is a sharp dip in reflected intensity and this phenomenon is called as surface plasmon resonance (SPR). The excitation of surface plasmons at the metal sensing layer interface has a wide range of applications in the field of biosensing [1–4]. Generally, Kretschmann configuration is used for SPR sensors where a p-polarised light at a particular wavelength is incident on coupling prism coated with metal [5]. At a specific combination of wavelength and angle of incidence, resonance occurs and a dip appears in the reflection spectrum. In the recent past, several SPR sensors have used graphene on the metal surface [6–8]. Graphene has a two-dimensional plane of carbon atoms arranged in a honeycomb-like lattice. It has optical conductivity from visible to infrared frequency due to the interband transition. Moreover, features such as high surface to volume ratio, broadband optical and plasmonic properties make it an appropriate candidate to be used as a functional coating material for existing plasmonic devices [9, 10]. Also, the high surface to volume ratio makes it suitable for adsorption of biomolecules in a large area. Moreover, the π orbitals of graphene form a dense cloud that blocks the gap within its atomic rings. This results in a repelling field which does not allow the molecules as small as helium to enter through it thereby preventing oxidation of metal surface [11–13]. It has been observed experimentally that graphene coated on surface of Au (111) adsorbs biomolecules (e.g. ssDNA) to a large extent due to π-stacking interaction between its hexagonal cells and the carbon-based atomic ring structures that are widely present in biomolecules [6]. But graphene-based gold-coated SPR sensors showed a broader SPR curve compared to graphene-based silver-coated SPR sensors [6, 8].

Although, graphene can be used on silver in Kretschmann configuration, the bulky arrangement makes it difficult to be used in remote sensing and online monitoring of refractive index. In order to achieve miniaturisation, several fibre-based SPR sensors have been reported [14–17]. Also, to couple light from core mode to plasmonic mode effectively, SPR sensors based on D-shaped fibre have been proposed [16, 18]. In case of conventional D-shaped fibre sensors, cladding has to be removed resulting in a significant loss of light via scattering effect. Moreover, in order to change the contrast of refractive index, doping of core is required. Nevertheless, the resonance wavelength cannot be easily tuned to the desired range of wavelength.

Photonic crystal fibres (PCF) have been used instead of conventional fibres for SPR-based sensors. The advantages such as controllable birefringence, tunable geometric parameters and low-temperature dependency have made it a better choice for SPR-based sensors [18–23]. Further, the effective index of the core-guided mode can be tailored by changing the geometrical parameters of the structure. This helps in phase matching of core-guided mode and plasmonic mode which is essential for SPR. In most of the abovementioned PCF-based SPR sensors, analyte to be detected has to be filled inside the voids of the fibre. However, it is difficult to remove or change the analyte present in the holes of the PCF.

In order to overcome the abovementioned difficulties, SPR sensor-based on D-shaped PCF has been proposed for refractive index (RI) sensing [24]. A D-shaped PCF can be fabricated by etching or side polishing the conventional PCF [25]. When cladding region comes closer to fibre after polishing, evanescent coupling from core guided modes occurs. Due to the proximity of the holes to the optical core, D-shaped PCF has a strong evanescent wave required for sensing. Moreover, it is easier to deposit metal on the flat surface than on the inner walls of holes of PCF. Most of the D-shaped PCF-based SPR sensors use gold or silver coating for sensing purpose [24, 26]. Zhixin Tan et al. [26] have reported gold-coated D-shaped hollow core PCF-based SPR sensor. Gold is chemically stable, and it shows large shifts in resonance wavelength. However, its absorption coefficient is larger which leads to broadening of resonance curve, and hence the performance deteriorates [27]. Moreover in this structure, liquid has to be filled in the core of the PCF which not only cause transmission loss but is cumbersome. As an alternative, silver can be used as plasmon active metal for sensing applications as it shows a sharper resonance peak compared to gold thereby increasing the detection accuracy. Ming Tian et al. have reported silver-coated D-shaped PCF sensor [24]. However, silver is prone to

oxidation which reduces the detection accuracy and direct adsorption of biomolecules (protein) on metal surface results in denaturalization of proteins and loss of their binding activity [11]. In order to overcome the abovementioned difficulties, we propose graphene-coated D-shaped PCF-based SPR sensor. The proposed structure is simple and easy from fabrication point of view. Compared to other carbon-based material, graphene has low cost and its synthesis is easier [28]. A single or few layers of graphene can be isolated and deposited on silver surface using several available techniques [11, 29]. Moreover, a number of graphene layers can be grown in a controlled manner because of the presence of van der Waals force between them [30]. Also, there is no need of filling the voids of the PCF, and hence the sensing is easier as the sensor can be used in a flow cell containing the analyte to be detected. The proposed sensor can be used to detect the change in RI of analyte as well as change in thickness of biolayer. However, the limitation of the proposed structure is that the biomolecules whose adsorption on graphene (due to similar type of bonding and structure) is high will result in better device performance. Further, reusability of the probe needs to be properly addressed as an error may occur in detection process if the analyte is not completely removed from the surface of probe. Figure 1 shows the proposed setup where light from a laser source is coupled to the D-shaped PCF and the transmitted light is coupled to the optical spectrum analyser for analysis.

Design Consideration and Theoretical Model

We used finite element method (FEM) to simulate the proposed structure. The cross-section of the D-shaped PCF is shown in Fig. 2. The whole section is divided into many triangular subdomains. The total number of mesh elements used for calculation is 220,202. The D-shaped structure can be fabricated from the full structure by widely available side polishing technique. The structure consists of two layers of holes. The holes in the second layer have a diameter of d_2= 1.4 µm. The four holes in the first layer have equal diameter of d_1=0.6 µm, while that of two others have different diameter. The two holes in the first layer have equal diameter as that of second layer holes. This helps in creating birefringence and coupling of a particularly polarised light with metal dielectric interface. The central hole helps in phase matching of the core-guided mode and plasmonic mode. The size of the central hole can also be tuned to shift the plasmonic resonance according to the availability of the source and detectors. The proposed structure is made up of silica, and all the holes in the structure

Fig. 1 Schematic diagram of the proposed experimental set-up

Laser source   Optics   Proposed PCF   Fiber port   OSA
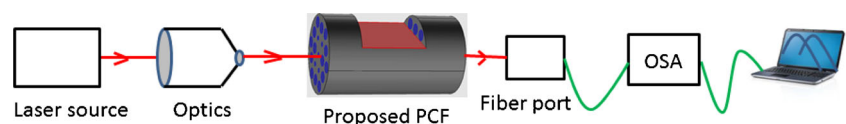
are air filled. The refractive index of silica is determined using Sellmeier equation [19].

$$n^2(\lambda) = 1 + \frac{A_1\lambda^2}{\lambda^2 - B_1} + \frac{A_2\lambda^2}{\lambda^2 - B_2} + \frac{A_3\lambda^2}{\lambda^2 - B_3} \qquad (1)$$

Where $A_1 = 0.696166300$, $A_2 = 0.407942600$, $A_3 = 0.897479400$, $B_1 = 4.67914826 \times 10^{-3}$ μm^2, $B_2 = 1.35120631 \times 10^{-2}$ μm^2 and $B_3 = 97.9340025$ μm^2. The thickness of silver layer deposited on the flat surface can be varied, and it is at a distance of $d_L = 2.7$ μm from the centre. The refractive index of silver in the proposed structure is taken from Palik [31]. The number of graphene layers is N. As each single layer has a thickness of 0.34 nm, the total thickness of graphene layer is $0.34 \times N$. The complex refractive index of graphene can be obtained using the equation

$$n = 3 + \frac{iC_1\lambda}{3} \qquad (2)$$

where $C_1 \approx 5.446$ μm^{-1} and λ is the vacuum wavelength [8, 32]. The maximum number of graphene layers considered for optimisation is five. When the number of graphene layers exceeds five, the electronic properties of graphene changes. The electronic bands of single-layer graphene split, and the infrared conductivity spectra converge towards the behaviour of bulk graphite [33].

Results and Discussion

Considering the above optimised parameters, a section of the proposed structure is used for the modal analysis due to its symmetrical nature. The modal analysis is done in XY plane while the propagation of light is along z direction as shown in Fig. 2. The two orthogonal lines are principal axis of the optical fibre. If the P wave component of the incident wave is aligned with the Y-axis of the optical fibre, then it interacts with the metal-sensing layer interface and at the same time S wave component simply propagates along X-axis [34]. Moreover, the birefringent nature of the proposed structure helps in better interaction of P wave component with the metal dielectric interface. Figure 3 shows the variation of real and imaginary part of effective indices of core-guided mode with wavelength of incident light. Resonance occurs when the real part of the effective index of the core-guided mode matches with that of plasmonic mode. The confinement loss depends on the imaginary part of the effective index and is given by $8.686 \times (2\pi/\lambda) \mathrm{Im}(n_{eff}) \times 10^4 \mathrm{dB/cm}$ where λ is in μm [21, 35]. The confinement loss is maximum, when the difference between the effective indices of core-guided mode and plasmonic mode is minimum. As can be seen from Fig. 3, the resonance occurs at $\lambda = 500$ nm where the loss is maximum. The inset figures (a) and (b) show the electric field profile of the core-guided mode and plasmonic mode, respectively. Further, the confinement loss plays an important role in analysing the performance of the sensor.

In order to study the performance of the sensor, analytes having a range of refractive indices are considered on the flat coated surface of the D-shaped structure. The refractive index of the analyte (n_a) is varied from 1.330 to 1.370 as shown in Fig. 4. As the refractive index of the analyte increases, the loss of the core-guided mode is found to increase and the peak corresponding to resonance shifts towards longer wavelength. This happens due to the fact that the change in refractive index of analyte affects the phase matching point between the core-guided mode and plasmonic mode. When the RI of analyte is

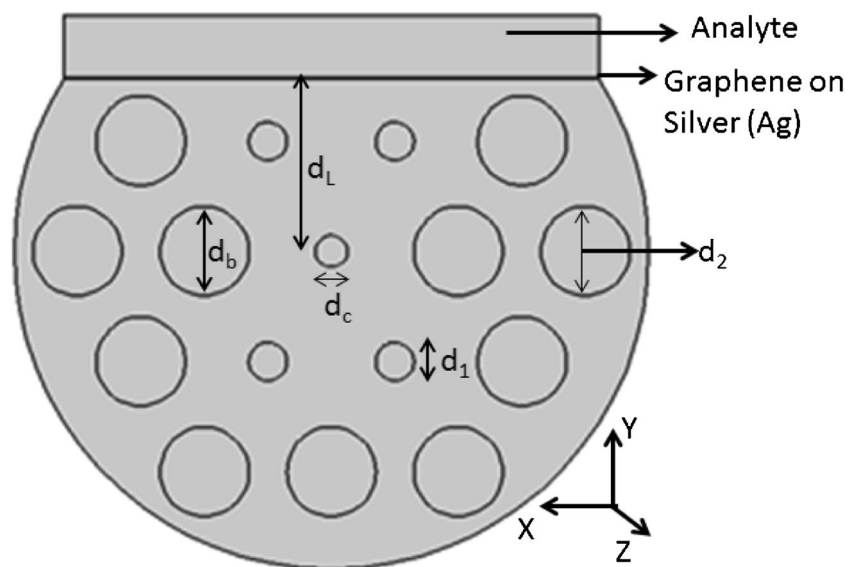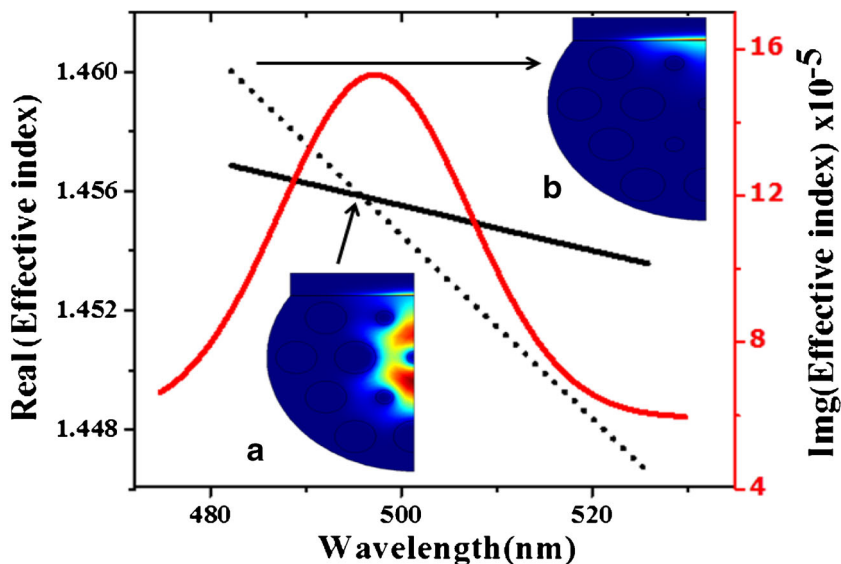Fig. 2 Schematic diagram of the proposed D-shaped PCF structure

Fig. 3 Dispersion relations of core-guided mode (*black solid line*), plasmonic mode (*black dotted line*) and imaginary part of core-guided mode (*red solid line*). Insets (*a*) and (*b*) show the electric field profile of core and plasmonic modes, respectively. The RI of analyte considered is 1.330

changed, the resonance condition is satisfied at a higher wavelength. This mechanism can be used for the detection of chemical analytes. Further, we have studied and optimised the performance of the sensor by investigating two important performance parameters: sensitivity and resolution. Generally, two types of interrogation methods such as amplitude interrogation and wavelength interrogation are used to determine the sensitivity of the sensor. In amplitude interrogation, all measurements are done at single wavelength. It is economical, and spectral manipulation is not required. However, it has lower sensitivity and smaller operational range than the wavelength interrogation process [19]. If P_0 is the power launched to the core mode of the fibre, then power detected after a propagation length of L is

$$P(L, \lambda, n_a) = P_0 e^{-\alpha(\lambda, n_a)L} \qquad (3)$$
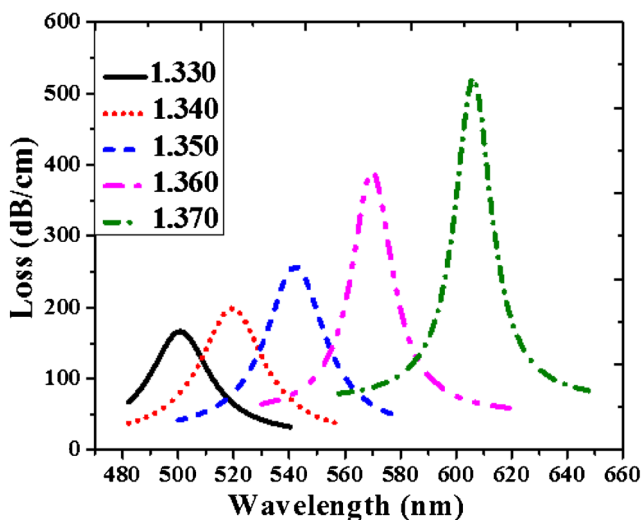
Fig. 4 Variation of transmission loss with wavelength for different refractive index of analyte

Where $\alpha(\lambda, n_a)$ is attenuation constant and is expressed as $\alpha = 2k_0 \mathrm{Im}(n_{\mathrm{eff}})$. The sensor length L is limited by modal transmission loss and is defined as $L = 1/\alpha(\lambda, n_a)$. For our case, the sensor length falls into subcentimeter range. The amplitude sensitivity can be calculated from the transmission loss of the core-guided mode. For a small change in refractive index of analyte, it is defined as [19]

$$S_A(\lambda)(\mathrm{RIU}^{-1}) = -(\partial\alpha(\lambda, n_a)/\partial n_a)/\alpha(\lambda, n_a) \qquad (4)$$

Using the abovementioned formula, we have optimised sensitivity of the proposed sensor by optimising several parameters like number of graphene layers, thickness of silver and diameter of central hole.

Amplitude Sensitivity with Number of Graphene Layers

Using Eq. (4), we first optimised the thickness of graphene keeping all other parameters like silver thickness, diameter of central hole as constant. The thickness of graphene layer can be varied by changing the number of layers. As the thickness of graphene layer increases, the peak corresponding to the resonance shifts towards longer wavelength. This happens due to the fact that increase in graphene thickness leads to increase in the effective index at the metal dielectric interface. So the resonance condition is satisfied at a higher wavelength. As can be seen from Fig. 5, the resonance wavelength $\lambda_{\mathrm{res}} = 502.54$ nm for monolayer of graphene while it is shifted to $\lambda_{\mathrm{res}} = 530$ nm for five layers of graphene. Further, the confinement loss of core mode due to the excitation of plasmonic mode decreased from 167 dB/cm for monolayer of graphene to 119 dB/cm for five layers of graphene, and the peaks broaden as can be seen from Fig. 5. This occurs due to the fact that the imaginary part of the dielectric constant of graphene leads
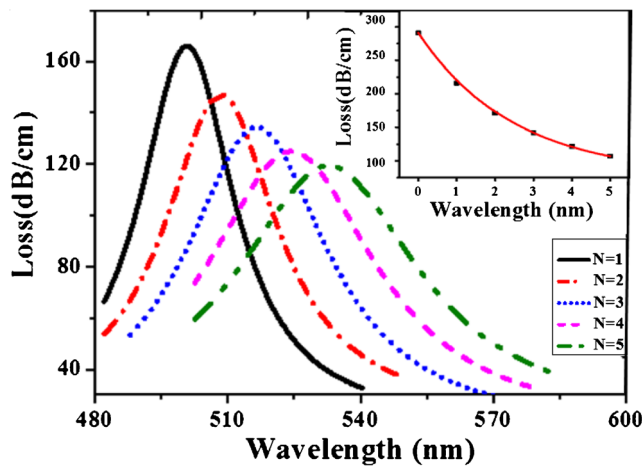
Fig. 5 Variation of transmission loss with wavelength for different number of graphene layers N varying from 1 to 5. *Inset* shows the variation of amplitude sensitivity with different number of graphene layers
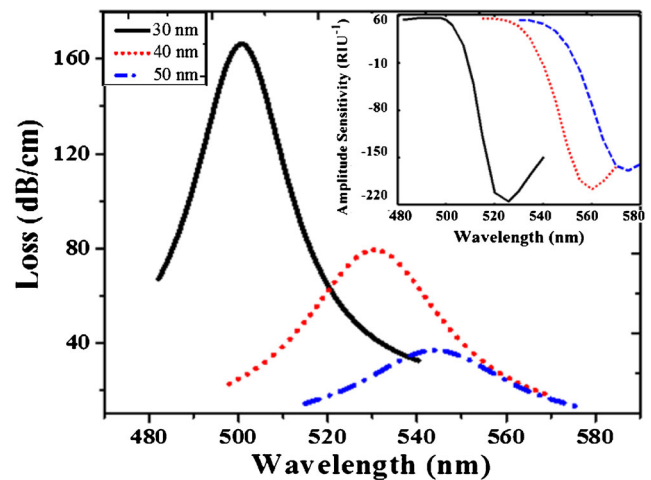

Fig. 6 Variation of transmission loss with wavelength for different thickness of silver layer varying from 30 to 50 nm. *Inset* shows the variation of amplitude sensitivity with wavelength for different silver

to damping loss. The damping loss increases with graphene thickness and the resonance curve broadens [26, 35]. In other words, the coupling of light from core mode to plasmonic mode decreases as most of the light is used in overcoming the damping effect of graphene. This leads to the less excitation of plasmonic mode, and hence the loss due to the excitation of plasmonic mode decreases. The decrease in loss leads to decrease in amplitude sensitivity as can be seen in the inset of Fig. 5. The sensitivity decreased from 216 RIU^{-1} (refractive index unit) for monolayer of graphene to 107 RIU^{-1} for five layers of graphene. Although the sensitivity of the sensor without graphene layer is higher, the oxidation of silver makes it difficult to be used effectively. So keeping the monolayer of graphene for better amplitude sensitivity, we optimised the thickness of metal layer.

Amplitude Sensitivity with Silver Thickness

Keeping monolayer of graphene on the silver surface, we varied the thickness of silver from 30 to 50 nm. As can be seen from Fig. 6, the transmission loss decreases from 167 dB/cm at 30 nm to 37 dB/cm at 50 nm of silver thickness and the peaks broaden with increase in silver thickness. With increase in silver thickness, damping loss increases. So most part of the core-guided mode is used in overcoming the damping loss, and hence the interaction of core mode with metal sensing layer interface decreases. Therefore, the loss occurring due to plasmonic mode decreases, and this decrease in loss leads to decrease in sensitivity. As can be seen from inset of Fig. 6, the sensitivity decreases from 216 RIU^{-1} at 30 nm to 170 RIU^{-1} at 50 nm of silver thickness. So the optimised silver thickness is taken as 30 nm.

Amplitude Sensitivity with Geometrical Parameters

Considering a monolayer of graphene and the optimised thickness of silver on the flat surface of PCF, we optimised the diameter of central hole which plays an important role in tuning the resonance wavelength. With the decrease in diameter of central hole, the interaction of the core-guided mode with the metal-sensing layer interface decreases, i.e. there is lesser expulsion of field from fibre core which in turn leads to the reduction in modal field at the metal dielectric interface. So the excitation of plasmon decreases leading to lower propagation loss. As can be seen from Fig. 7, the loss is 167 dB/cm for the central hole having a diameter d_c=0.5 μm, while that with d_c=0 is 38 dB/cm. Moreover, as the effective index of the
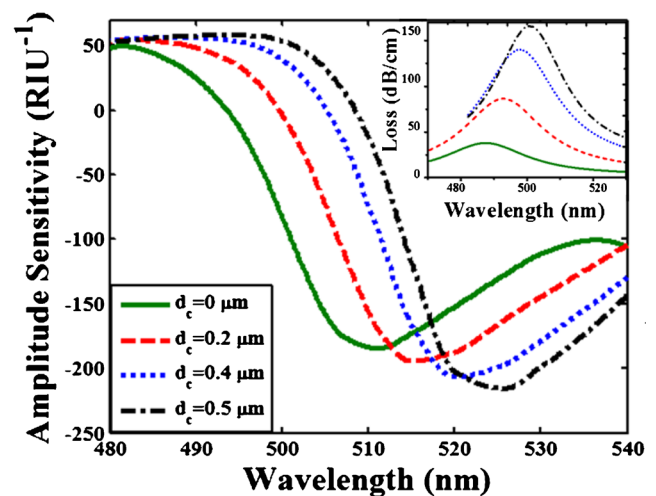

Fig. 7 Variation of amplitude sensitivity with wavelength of incident light for diameter of central hole varying from 0 to 0.5 μm. *Inset* shows the corresponding variation of transmission loss with wavelength of the incident light

mode at the centre increases with decrease in size of air hole, the plasmon peak shifts towards shorter wavelength in order to satisfy the resonance condition. The reverse shift occurs in case of increase in size of central hole. Further, the decrease in loss leads to a decrease in amplitude sensitivity from 216 RIU^{-1} at d_c=0.25 µm to 175 RIU^{-1} at d_c=0 µm as can be seen from Fig. 7. Moreover, one may further optimise the structure by varying the diameter of holes responsible for birefringence.

We varied the diameter of bigger holes in the first layer responsible for birefringence in order to further optimise the geometry of the structure. As we decrease the diameter of holes from 1.4 to 0.6 µm, the interaction of y-polarised light with the metal-sensing layer interface decreases. So the corresponding loss decreases which leads to decrease in sensitivity. As can be seen from Fig. 8, the sensitivity decreased from 216 RIU^{-1} for d_b=1.4 to 197 RIU^{-1} for d_b=0.6 µm. Further, we have optimised the polishing depth (d_L) of the proposed structure. We considered three values of d_L (2.5, 2.6, 2.7 µm) for the analysis of the performance of the sensor as for higher values of d_L, the dispersion loss will be more while lower value of d_L will affect the structure and stability of the fibre. As can be seen from Fig. 9, the sensitivity does not get affected with slight variation in polishing depth.

Amplitude Sensitivity with Optimised Parameters

Considering all the above optimised parameters, we compared the sensitivity of the proposed graphene-coated silver-based sensor with gold-coated silver as gold can also be used to prevent the oxidation of silver. We took a thin layer of gold having a thickness of 5 nm on silver. As can be seen from Fig. 10, the sensitivity decreases from 216 RIU^{-1} for graphene-coated silver to 160 RIU^{-1} for gold-coated silver.

Fig. 9 Variation in amplitude sensitivity with wavelength of the incident light for different polishing depth (d_L) varying from 2.5 to 2.7 µm

This happens due to more damping of light in gold. Moreover, deposition of very thin layer of gold leads to the formation of island, while a thin layer of graphene can easily be deposited on the surface of silver. So considering monolayer of graphene on silver, we calculated the resolution of the sensor. If 1 % change in transmitted intensity can be detected reliably, then the sensor resolution becomes 4.6×10^{-5} RIU. Moreover, if the structure is modified to reduce the loss, then it will lead to the reduction in sensitivity. Therefore, there is a trade of between loss and sensitivity which can be optimised as per the requirement.

Wavelength Interrogation

In wavelength interrogation, the transmission spectra are analysed before and after the change in analyte refractive index [19]. The change in refractive index of analyte is detected
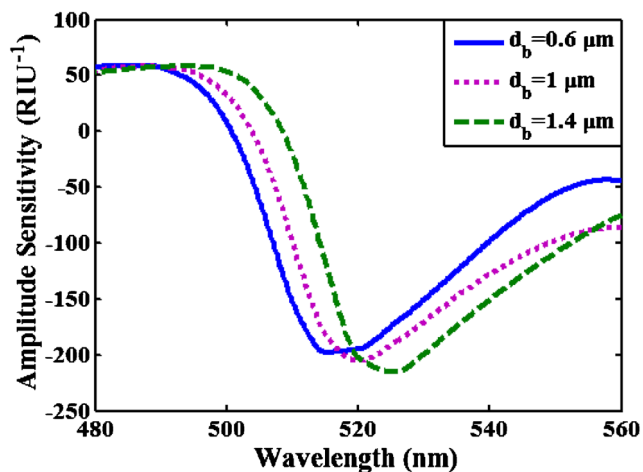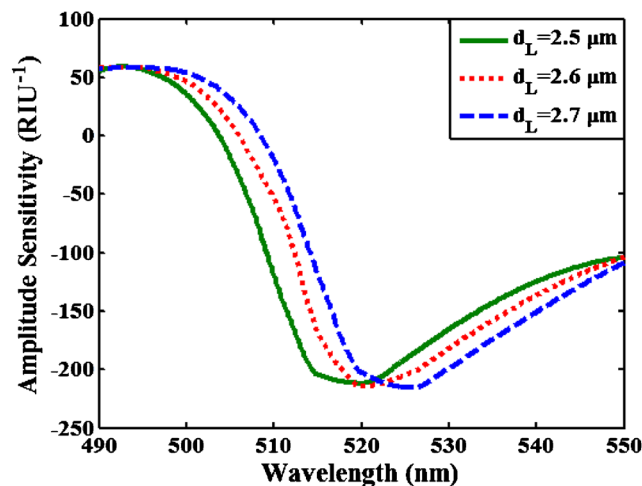

Fig. 8 Variation of amplitude sensitivity with wavelength of the incident light for different diameter of holes (d_b) responsible for birefringence. The value of d_b varies from 0.6 to 1.4 µm
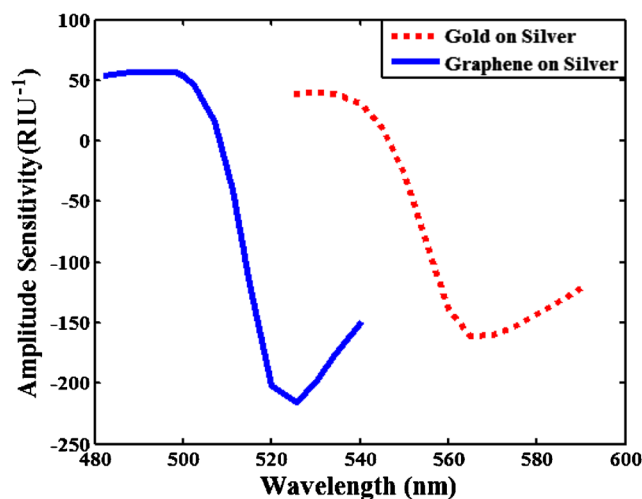

Fig. 10 Comparison of amplitude sensitivity of gold-coated silver and graphene-coated sensors

by measuring the shift in the resonance peak. This type of interrogation has a larger operational range, and it is more sensitive than that of amplitude interrogation. The wavelength sensitivity is defined as $S_\lambda(\text{nm/RIU}) = \left| \frac{d\lambda_{\text{peak}}}{dn_a} \right|$. For the proposed sensor, the peak of the resonance curve shifted towards higher wavelength with increase in refractive index of analyte as shown in Fig. 4. Further, with increase in RI of analyte, the shift in resonance wavelength is exponential as can be seen from Fig. 11. The sensitivity is found to be as high as 3700 nm/RIU for an analyte refractive index of 1.360. Further, the resolution of a sensor is defined as $R = \Delta n_a \frac{\Delta\lambda_{\text{min}}}{\Delta\lambda_{\text{peak}}}$, where $\Delta\lambda_{\text{peak}}$ = shift in the resonance peak, Δn_a = change in refractive index of analyte, $\Delta\lambda_{\text{min}}$ = minimum shift detectable by the detector. If the instrumental resolution is assumed to be $\Delta\lambda$=0.1 nm, the refractive index resolution of the corresponding sensor is 2.7×10^{-5} RIU which is comparable to the resolution available in the market.

Application in Biosensing

Considering the advantages of graphene in biomolecular detection, the proposed sensor can be used for detection of thickness of biolayer. Proteins (antibodies) have a diameter of 4–10 nm, and these antibodies also help in capturing specific kind of target proteins by lock key mechanism [36]. Thickness of biomolecules using gold-coated PCF surface has been reported earlier [36]. However, denaturalisation of protein occurs when it is deposited on metals like gold and silver. [11]. In our proposed structure, graphene on silver surface helps not only in preventing oxidation of silver but also helps in adsorption of biomolecules.

The sensitivity in case of SPR-based biosensors is determined by its capability to detect the change in thickness of
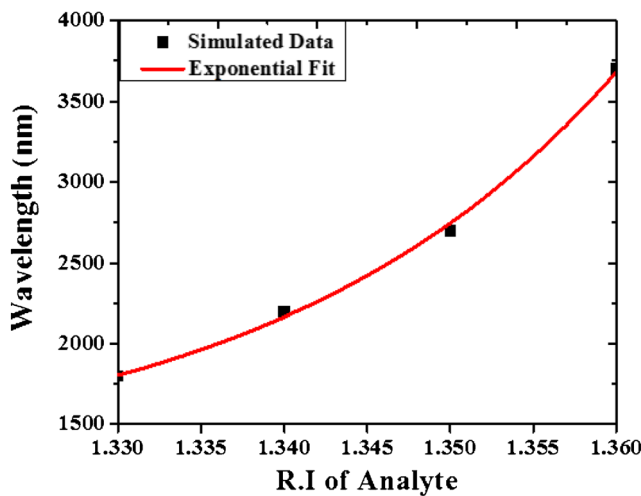
biolayer on top of a metal film. The refractive index of biolayer generally varies between 1.400 and 1.420 for most of the biomolecules [36]. A thin layer of biolayer on graphene followed by analyte having refractive index equal to that of water (1.330) is considered for analysis. Taking the above factors, the loss of the core-guided mode as function of wavelength for a range of biolayer thickness is plotted in the inset of Fig. 12. As can be seen from the figure, the loss increases from 166 dB/cm for no biolayer to 295 dB/cm for biolayer thickness of 25 nm. Moreover, with increase in biolayer thickness, the peak shifts towards higher wavelength. We plotted the change of position of peak with increase in thickness of biolayer in the inset of Fig. 12. For a change in biolayer thickness of 10 nm, the peak of loss curve is shifted by 20 nm and the shift of peak increases linearly with change in thickness as can be seen from Fig. 12. This mechanism can be used to monitor biolayers having thickness in the range of nanometers. In wavelength interrogation, the sensitivity for thickness of biolayer is defined as [36]

$$S = \frac{d\lambda_{\text{peak}}}{dT_b} \tag{5}$$

Where $d\lambda_{\text{peak}}$ = shift in peak corresponding to resonance and dT_b=change in thickness of biolayer. As can be noted from Fig. 12, the shift in peak $d\lambda$ is 20 nm which leads to a spectral sensitivity of 2. If 0.1 nm change in the position of the peak can be detected, then a resolution of 50 pm is achievable.

Moreover, the amplitude interrogation can also be used to calculate the sensitivity for change in biolayer thickness. In
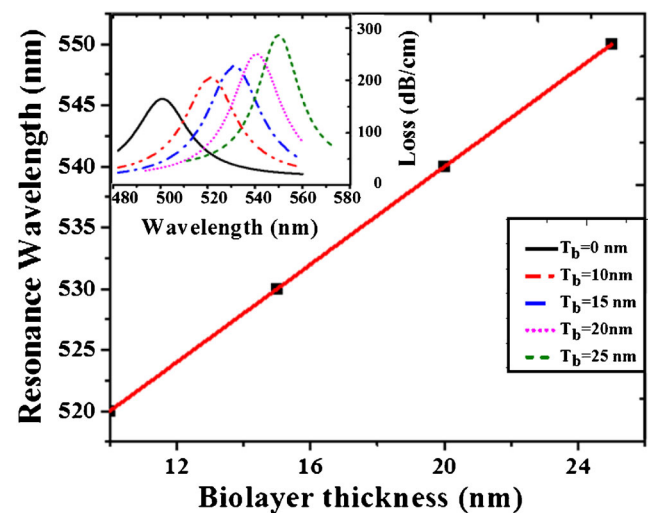

Fig. 11 Variation of wavelength sensitivity with change in refractive index of analyte varying from 1.330 to 1.360

Fig. 12 Variation of resonance wavelength with thickness of biolayer having refractive index of 1.420. *Inset* shows the variation of loss of the fundamental core mode for without biolayer and biolayer with varying thickness

amplitude interrogation, the sensitivity for thickness is defined as [36]

$$S_A = -\left(\frac{\partial \alpha(\lambda, d_{\text{bio}})}{\partial d_{\text{bio}}}\right) \frac{1}{\alpha(\lambda, d_{\text{bio}})} \quad (6)$$

As can be seen from Fig. 13, the amplitude sensitivity reaches a maximum of 0.26 nm^{-1} at a wavelength of 525 nm. So the transmitted intensity will be changed by 26 % for 1-nm change in thickness of biolayer. If 1 % change in transmitted intensity can be detected, then resolution of 39 pm is achievable. Therefore, the proposed structure can be effectively used as a biosensor in both amplitude and wavelength interrogation depending upon the requirement.

Conclusion

A graphene-coated D-shaped PCF-based plasmonic sensor has been proposed. Finite element method (FEM) has been used for calculation. The whole structure is divided into large number of triangular subdomains. Silver has been used as the plasmonic metal for the proposed structure, and graphene helps in the prevention of oxidation of silver surface. Moreover, the use of graphene leads to the absorption of biomolecules due to the π-π stacking interaction between hexagonal cells of graphene and the carbon-based atomic ring structures that are widely present in biomolecules. The sensor can detect thickness of biolayers like antibodies as well as refractive index of biochemical analytes. Further, it can be used for both amplitude and wavelength interrogation process. The results show that it has an amplitude sensitivity of 216 RIU^{-1} with resolution of 4.6×10^{-5}. The spectral sensitivity has been found to be as high as 3700 nm/RIU with the resolution of
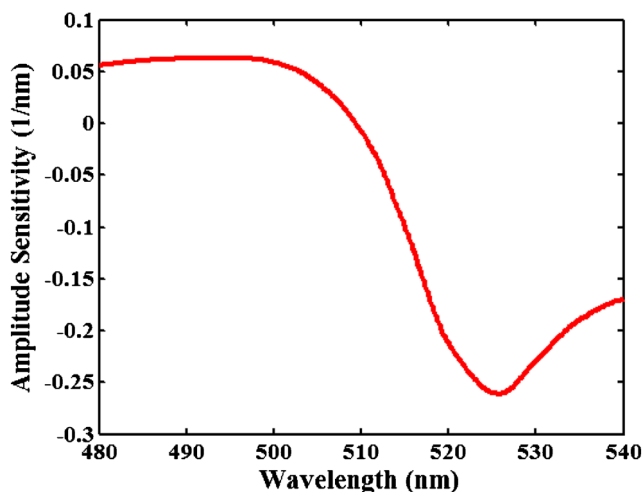
the sensor as 2×10^{-5}. Moreover, a resolution of 39 pm for determination of biolayer thickness in amplitude interrogation method and 50 pm for the same in spectral interrogation scheme can be achieved. Riding on the advantages of latest nanofabrication technique and commercial synthesis of few layers of graphene, the proposed structure can be used for a wide range of applications.

Compliance with Ethical Standards The consent has been taken from the other author.

References

1. Wijaya E, Lenaerts C, Maricot S, Hastanin J, Habraken S, Vilcot J-P, Boukherroub R, Szunerits S (2011) Curr Opinion Solid State Mater Sci 15:208–224
2. Oh G-Y, Lee T-K, Kim H-S, Kim DG, Choi Y-W (2012) Opt Exp 20: 19067–19074
3. Koubova V, Brynda E, Karasova L, Skvor J, Homola J, Dostalek J, Tobiska P, Rosicky J (2001) Sensors Actuators B Chem 74:100–105
4. Homola J, Dostalek J, Chen SF, Rasooly A, Jiang S, Yee SS (2002) Int J Food Microbiol 75:61–69
5. Kretchmann E, Raether ZH (1968) Z Naturforsch Phys Sci 23A: 2135–2136
6. Wu L et al (2010) Opt Exp 18:14395–14399
7. Maharana PK, Srivastava T, Jha R (2014) J Phys D Appl Phys 47: 385102-1–385102-11
8. Choi SH, Kim YL, Byun KM (2011) Opt Exp 19:458–466
9. Nair RR, Blake P, Grigorenko AN, Novoselov KS, Booth TJ, Stauber T, Peres NMR, Geim AK (2008) Science 320:1308
10. Wu Z et al (2013) IEEE Sensors J 13:777–782
11. Salihoglu O, Balci S, Kocabas C (2012) Appl Phys Lett 100:1–5
12. Berry V (2013) Carbon 62:1–10
13. Scott Bunch J, Verbridge SS, Alden JS, van der Zande AM, Parpia JM, Craighead HG, McEuen PL (2008) Nano Lett 8:2458–2462
14. Jha R, Badenes G (2009) Sensors Actuators A 150:212–221
15. Verma R, Srivastava SK, Gupta BD (2012) IEEE Sensors J 12:3460–3466
16. Kim JA, Hwang T, Reddy S, Dugasani, Amin R, Kulkarni A, Park SH, Kim T (2013) Sensors Actuators B Chem 187:426–433
17. Perrotton C et al (2011) Opt Exp 19 A:1175–1183
18. Chen C-H, Tsao T-C, Tang J-L, Wei-Te W (2010) Sensors 10:4794–4804
19. Akowuah EK, Gorman T, Ademgil H, Haxha S, Robinson GK, Oliver JV (2012) IEEE J Quantum Electron 48:1403–1410
20. Yu X, Zhang Y, Pan S, Shum P, Yan M, Leviatan Y, Li C (2010) J Opt 12:1–4
21. Dash JN, Jha R (2014) IEEE Photon Technol Lett 26:595–598
22. Villatoro J, Kreuzer MP, Jha R, Minkovich VP, Finazzi V, Badenes G, Pruneri V (2009) Opt Exp 17:1447–1453
23. Dash JN, Jha R (2014) IEEE Photon Technol Lett 26:1092–1095
24. Ming T, Lu P, Chen L, Lv C, Liu D (2012) Opt Comm 285:1550–1554
25. Kim HJ, Kown OJ, Lee SB, Han Y-G (2011) Appl Phys B 102:81–85
26. Tan Z, Li X, Chen Y, Fan P (2013) Plasmonics. doi:10.1007/s11468-013-9609-8
27. Maharana PK, Srivastava T, Jha R (2013) IEEE Photon Technol Lett 25:122–125

Fig. 13 Variation of amplitude sensitivity of the proposed sensor to the change in biolayer thickness

28. Hernandez FJ, Ozalp VC (2012) Biosensors 2:1–14
29. Liang X, Fu Z, Chou SY (2007) Nano Lett 7:3840–3844
30. Dappe YJ, Basanta MA, Flores F, Ortega J (2006) Phys Rev B 74: 205434, 1–9
31. Palik ED (1985) Academic Press, San Diego
32. Bruna M, Borini S (2009) Appl Phy Lett 94:031901
33. Mak KF, Sfeir MY, Misewich JA, Heinz TF (2010) PNAS 107: 14999–15004
34. Lo Y-L, Chuang C-H, Lin Z-W (2011) Opt Lett 36:2489–2491
35. Ying D, Shu-Guang L, Shuo L (2012) Chin Phys B 21:1–6
36. Hassani A, Skorobogatiy M (2009) J Opt Soc Am B 26:1550–1557